Journal of
Materials Chemistry C

PAPER

View Article Online
View Journal | View Issue

Cite this: J. Mater. Chem. C, 2016, 4, 5073

Columnar liquid-crystalline assemblies of X-shaped pyrene–oligothiophene conjugates: photoconductivities and mechanochromic functions†

Kian Ping Gan, Masafumi Yoshio* and Takashi Kato*

Received 25th February 2016,
Accepted 8th April 2016

DOI: 10.1039/c6tc00808a

www.rsc.org/MaterialsC

π-Conjugated liquid crystals have great potential as organic semiconductors owing to their smooth thin-film forming and flexible properties, as well as charge carrier transport ability. In the present study, we have designed and synthesised X-shaped columnar liquid crystals with pyrene as the central core, which are fourfold conjugated with bithiophene moieties, and tethered with eight or twelve alkoxy chains at their extremities. These X-shaped molecules show hexagonal, tetragonal, and rectangular columnar liquid-crystalline (LC) phases over a wide range of temperature. The extended π-conjugation has led to the realisation of a moderately low bandgap. The hole mobilities of both molecules in their various LC states are revealed to be in the order of 10^{-4} to 10^{-5} cm^2 V^{-1} s^{-1} using the time-of-flight (TOF) photoconductivity measurements. In addition, the mechano-responsive photoluminescent change has been observed for the columnar phase of the X-shaped molecule with eight alkoxy chains. The possible π-stacking configurations are discussed. The introduction of a gelator, *N*,*N*′-bis(lauroyl)-hydrazine, into the X-shaped molecules leads to the formation of a LC gel that produces a change in the measured hole mobility. The presented strategy could lead to the design of new solution-processable, low bandgap semiconducting materials for optoelectronic devices.

Introduction

π-Conjugated liquid crystals have attracted considerable attention because of their ease of molecular alignment and anisotropic charge carrier transport ability.[1–4] Since the early reports of carrier transport of triphenylenes in the columnar phases by Boden, Haarar, and Ringsdorf *et al.*,[5,6] a variety of columnar liquid crystals that show charge carriers transport have been reported.[7–30] Polycyclic aromatic hydrocarbon derivatives such as perylene, pyrene, and other heteroaromatic molecules including phthalocyanine and fused thiophene have come under intense scrutiny because of their potential to be employed as mesogenic cores. These columnar liquid-crystalline (LC) π-conjugated molecules have found applications in organic optoelectronic devices such as organic light emitting diodes (OLEDs),[31,32] organic field-effect transistors (OFETs),[33–35] and organic photovoltaics (OPVs).[36–39] As such, π-conjugated columnar liquid crystals are emerging as promising semiconducting soft materials due to their abilities to form one-dimensional π–π columnar stacks that allow high charge carrier transport and their capabilities to form smooth thin films with a uniaxially oriented columnar domain, which are essential for optimal device performance.

Oligothiophene derivatives are promising for applications in electronics because of their charge transport abilities and fluorescence properties. Smectic and nematic LC oligothiophenes are intensively studied,[40–48] however the examples of the columnar LC assembly of oligothiophene are limited. We previously reported on the first example of columnar LC polycatenar oligothiophenes (Scheme 2) with electronic and photonic functions,[49,50] and helical stacking of propeller-shaped oligothiophene-triazine conjugates in columnar LC phases that results in ambipolar charge transport.[51] In addition, we developed mechanochromic liquid crystals containing π-conjugated chromophores such as pyrene and oligothiophene as their central cores.[52–56] The luminescent colours vary by mechanical stimuli, which are attributed to the change in the LC molecular assembled structures between the columnar and cubic LC phases. However, LC molecules that exhibit both charge transport properties and mechanochromic functions have not been explored. If these properties could be realised, a new class of supramolecular optoelectronic materials could be created with possible applications

Department of Chemistry and Biotechnology, School of Engineering, The University of Tokyo, Hongo, Bunkyo-ku, Tokyo 113-8656, Japan. E-mail: yoshio@chembio.t-u-tokyo.ac.jp, kato@chiral.t.u-tokyo.ac.jp; Fax: +81-3-5841-8661; Tel: +81-3-5841-7440

† Electronic supplementary information (ESI) available: Experimental, molecular modelling, thermogravimetric curves, DSC traces, POM images and XRD patterns, lattice analyses, transient photocurrent curves, UV-vis and fluorescence spectra, POM/SEM images and hole mobilities of LC gels. See DOI: 10.1039/c6tc00808a

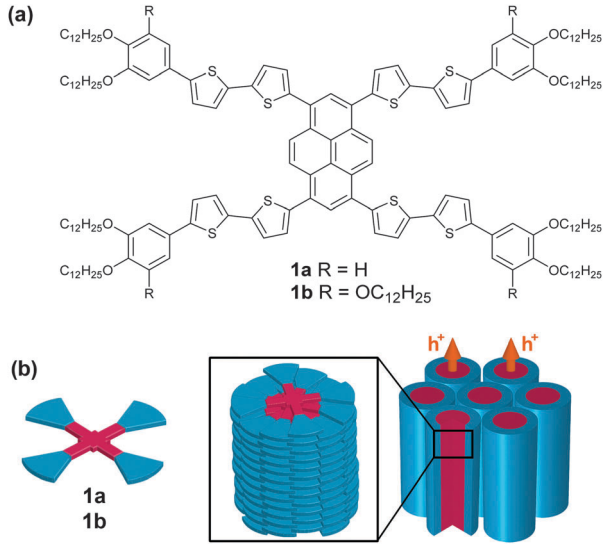

Fig. 1 The molecular structure of the X-shaped molecules with a π-conjugated core (a), and the one-dimensional π–π columnar stacks that facilitate charge transport (b).

to displays, memory devices, and sensors.[57–60] We envisaged that the combination of rod-shaped oligothiophenes with a disc-like pyrene would produce a multi-functional neoteric columnar liquid crystal that could exhibit both charge carrier transport and stimuli-responsive photoluminescent properties.

Herein, we report X-shaped molecules **1a** and **1b** (Fig. 1a) consisting of intercrossing polycatenar oligothiophenes through a central pyrene core (see ESI,† Fig. S1 for molecular modelling). The X-shaped molecules can form hole-transporting columnar LC phases *via* one-dimensional stacks (Fig. 1b). The molecular stacks are also tunable by the application of mechanical shear force, inducing a change in photoluminescence colour.

Results and discussion

Synthesis and characterisation

The X-shaped pyrene–oligothiophene conjugates **1a** and **1b** were synthesised according to the synthetic route shown in Scheme 1 (see ESI,† Section S1 for detailed experimental procedures). The Suzuki–Miyaura cross-coupling reaction of alkoxy bromobenzene **2a** with 2,2′-bithiophene-5-boronic acid pinacol ester yielded **3a**, which is then followed by an iridium-catalysed borylation reaction[61] with bis(pinacolato)diboron to afford the corresponding pinacol ester **4a**. The fourfold Suzuki–Miyaura cross-coupling reaction of **4a** with 1,3,6,8-tetrabromopyrene afforded the desired X-shaped molecule **1a**. Compound **1b** was obtained by the identical synthetic pathway. Both X-shaped molecules **1a** and **1b** were characterised and verified by ^{1}H and ^{13}C NMR spectroscopy, MALDI-TOF mass spectrometry, and elemental analyses.

Compounds **1a** and **1b** are highly soluble in organic solvents like hexane, toluene, dichloromethane, chloroform, and THF. Both compounds exhibit a high thermal stability of above 300 °C under air (see ESI,† Fig. S2). As such, these molecules could be processed and annealed under air without extensive oxidative decomposition.

Liquid-crystalline properties

The thermotropic LC properties and X-ray diffraction (XRD) data of the X-shaped molecules **1a** and **1b** are summarised in Table 1 (see ESI,† Fig. S3 for DSC thermograms). The polarising optical microscopic (POM) textures and XRD patterns are shown in Fig. 2 (see ESI,† Fig. S4 for additional POM images and XRD patterns). Compound **1a** with 8 alkoxy chains at the peripheries exhibits enantiotropic hexagonal columnar phases (Col_h). Observations under the POM show that **1a** exhibits a fan-shaped texture with a large domain size when cooled from the isotropic melt at a rate of less than 1 °C min^{-1} (Fig. 2a). The wide angle X-ray diffraction (WAXD) pattern at 125 °C shows two peaks at 40.7 (100) and 20.0 Å (200) (Fig. 2b). In addition, the two- dimensional small angle X-ray diffraction (SAXD) pattern at the same temperature reveals diffraction spots with a six-fold symmetry at the (100) plane (Fig. 2c), indicating a Col_h phase, with an intercolumnar distance of 47.0 Å (see ESI,† Fig. S5a and b). When **1a** is cooled to below 117 °C, at which the DSC chart on a cooling process exhibits an exothermic peak, no visible change in the texture is seen (see ESI,† Fig. S4a). At 100 °C, the WAXD pattern of **1a** shows three diffraction peaks at 43.2 (100), 21.2 (200), and 13.8 Å (300) (see ESI,† Fig. S4b) with a

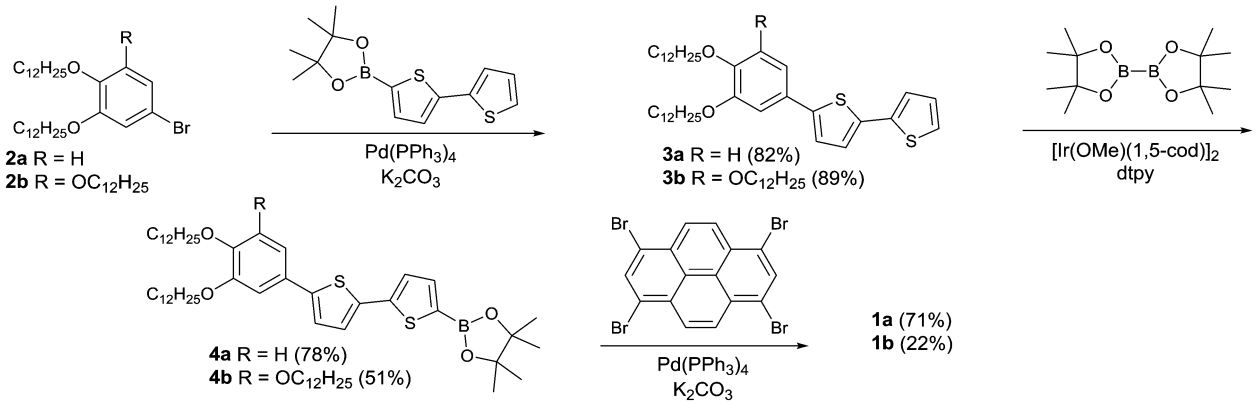

Scheme 1 The synthetic scheme of the X-shaped pyrene-bithiophene conjugates **1a** and **1b**.

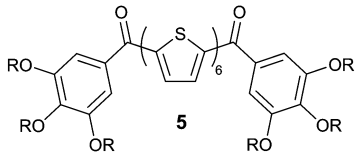

5

Scheme 2 The polycatenar oligothiophene derivative **5** previously reported.[49,50]

Table 1 Phase transition thermal properties and XRD data for **1a** and **1b**

Compound	Phase transition behaviour[a]			XRD data T/°C	Lattice parameters/Å
1a	G 20 Col_{h1}	117 Col_{h2} (26)	132 Iso (1)	125	a = 47.0
				100	a = 49.9
1b	Col_{r1} 10 Col_{r2} (43)	100 Col_t (12)	135 Iso (6)	125	a = 40.3
				90	a = 75.8
					b = 52.0
				−5	a = 68.8
					b = 47.9

[a] Transition temperatures (°C) and transition enthalpies (kJ mol^{-1}) in parentheses, determined by DSC on cooling at a rate of 10 K min^{-1}. G, glassy; Iso, isotropic; Col_h, hexagonal columnar phase; Col_t, tetragonal columnar phase; Col_r, rectangular columnar phase. Subscript numbers 1 and 2 indicate first and second columnar phases, respectively.

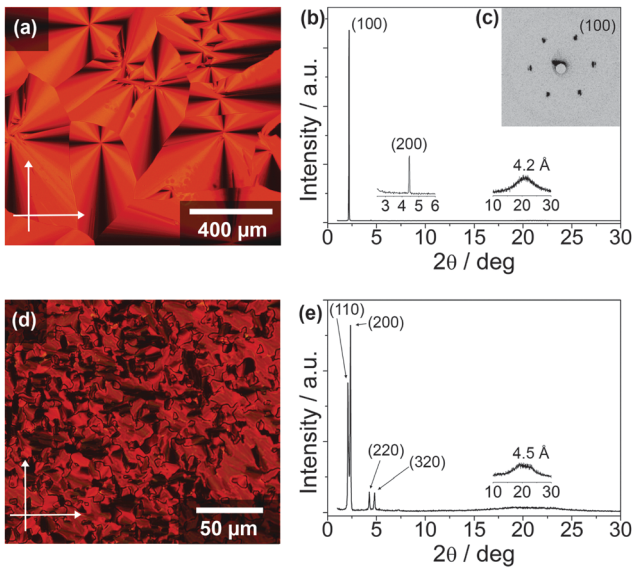

Fig. 2 POM photographs (left panels) and WAXD patterns (right panels). Compound **1a** in the Col_{h2} phase at 125 °C (a and b) with its SAXD pattern at the same temperature (c). Compound **1b** in the Col_{r2} phase at 90 °C (d and e).

lattice parameter a of 49.9 Å. Furthermore, the two-dimensional SAXD pattern of **1a** at 100 °C also exhibits a hexagonal symmetry at the (100) plane (see ESI,† Fig. S4c). These results suggest a transition from the Col_{h2} to a new Col_{h1} phase. The larger intercolumnar distance can be attributed to a change in the cofacial stacking configuration (*vide infra*), as well as more extended and rigid alkyl chains of the Col_{h1} phase as compared to that of the Col_{h2} phase. A transition to a glassy state is seen when **1a** is cooled to below 20 °C.

Compound **1b** with 12 alkoxy chains at the peripheries exhibits a similar isotropic transition temperature to **1a** upon heating. Cooling from the isotropic melt reveals a polydomain texture of **1b** at 125 °C (see ESI,† Fig. S4d). The WAXD and SAXD patterns of compound **1b** at 125 °C show diffraction peaks at 40.3 (100), 29.3 (110), 19.6 (200), and 14.9 Å (300) (see ESI,† Fig. S4e and f), which indicate a tetragonal columnar (Col_t) phase (see ESI,† Fig. S5c). The texture of **1b** (Fig. 2d) remains relatively unchanged upon cooling to below 100 °C as compared to the texture observed at 125 °C. However, the WAXD pattern is significantly different with four distinct peaks at 42.9, 37.9, 20.7, and 18.4 Å (Fig. 2e) observed at 90 °C, which correspond to the diffractions from the (110), (200), (220), and (320) planes of a rectangular columnar phase (Col_r) with a $P2_1/a$ symmetry (see ESI,† Fig. S6a and S7). Using the Debye Scherer method, the lattice parameters a and b are evaluated to be 75.8 and 52.0 Å, respectively (see ESI,† Fig. S6a). Further cooling of **1b** to below 10 °C induced a transition to a new Col_r phase (Col_{r2} to Col_{r1} phase), with the lattice parameters a and b of 68.8 and 47.9 Å, respectively (see ESI,† Fig. S4g, h and S6b).

Hole carrier transport

The time-of-flight (TOF) photoconductivity method was used to examine the hole mobilities of compounds **1a** and **1b**. The samples form LC domains oriented parallel to the surface of the indium-tin-oxide (ITO) cells with a sample thickness of 9 μm by slow cooling from isotropic states to room temperature.

Compounds **1a** and **1b** illuminated by a pulsed YAG laser at 355 nm under applied electric fields at room temperature show non-dispersive transient photocurrent curves of hole carriers (see ESI,† Fig. S8). The transit time is taken at the inflection point of the photocurrent curves. The hole mobilities measured are nearly independent of the applied voltage, which is the characteristic feature for charge carrier transport of semiconductors.[40]

Temperature dependence of the hole carrier mobilities of **1a** and **1b** is shown in Fig. 3. Compound **1a** in the isotropic state shows hole mobilities in the order of 10^{-5} cm^2 V^{-1} s^{-1}. The transition from the isotropic state to the Col_{h2} phase induces an increase in the hole mobility. The maximum value in the Col_{h2} phase of **1a** at 117 °C is 4.4 × 10^{-4} cm^2 V^{-1} s^{-1}. This increment in the hole mobility can be attributed to the facilitation of charge carrier transport due to the formation of the one-dimensional π–π columnar stacks. In the Col_{h1} phase of **1a**, the hole mobilities slightly decrease with decreasing temperature.

As for compound **1b**, an abrupt increase of the hole mobilities is observed at the Iso to Col_t transition. The maximum value of 2.3 × 10^{-4} cm^2 V^{-1} s^{-1} is observed at 130 °C in the Col_t phase. The hole mobilities of **1b** in the Col_t phase decrease by approximately one order of magnitude with decreasing temperature. In the Col_{r2} phase, no significant change in the hole mobilities is observed with varying temperature.

Mechanochromic properties

The stimuli-reponsive properties of the X-shaped molecules **1a** and **1b** were explored. Under the irradiation of UV light, the luminescence colour of compound **1a** changes from red to

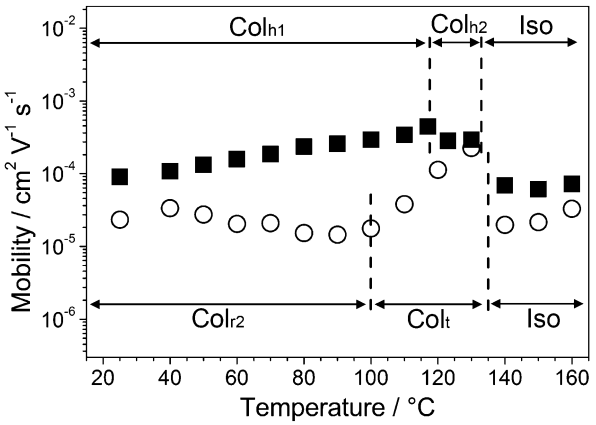

Fig. 3 The logarithmic plot of hole mobilities of **1a** (■) and **1b** (○) as a function of temperature on cooling. Dotted lines denote phase transition temperatures.

orange when a mechanical shear force is applied on the sample in the Col_{h1} phase at room temperature (Fig. 4), forming a new disordered Col phase (*vide infra*). The red luminescence of the initial state (Col_{h1} phase) of **1a** is recovered by heating the sheared sample to the isotropic state and then cooling to room temperature. In contrast, compound **1b** shows no apparent difference in luminescence colour before or after shearing (see ESI,† Fig. S9).

To clarify the photophysical properties of **1a** before and after mechanical shearing, UV-vis absorption (Fig. 5a, left) and photoluminescence spectra (Fig. 5a, right) of **1a** have been measured on quartz substrates at ambient temperature. In addition, in the isotropic liquid phase at 150 °C and the Col_{h2} phase at 125 °C of **1a**, the UV-vis absorption and emission spectra (Fig. 5b) have also been taken for comparison with those of the shear-induced phase.

The absorption spectra of **1a** (Fig. 5a, left) show three absorption peaks (Fig. 5, left). The two absorption peaks with higher energy wavelengths at around 364 and 414 nm can be ascribed to the $\pi \rightarrow \pi^*$ transition from the oligothiophene-conjugated pyrene core, while the absorption peak with lower energy wavelength at around 505 nm is probably due to $n \rightarrow \pi^*$ from the sulfur heteroatom of the thiophene moiety.[62] No significant differences in the absorption spectra before and after shearing are observed (Fig. 5a, left), although the absorption edge of the shear-induced phase is slightly blue-shifted to that of the Col_{h1} phase. In contrast,

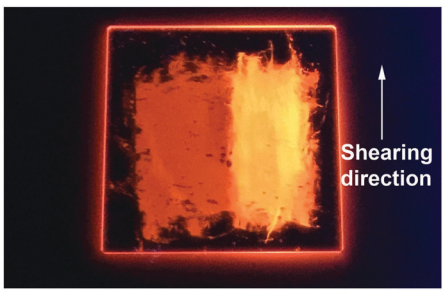

Fig. 4 The photograph of **1a** at room temperature on a quartz plate under illumination of UV light (365 nm) for the original Col_{h1} sample (left half) and the sheared sample (right half).

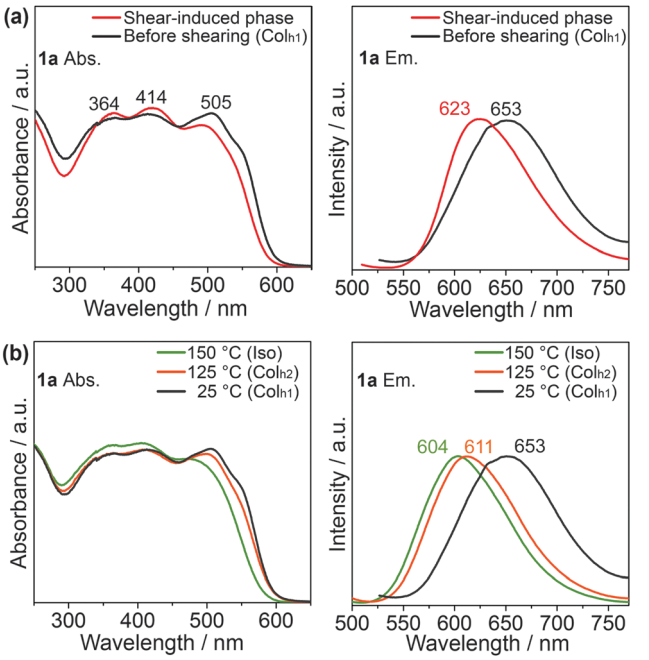

Fig. 5 The normalized UV-vis absorbance (left panels) and emission (right panels) spectra (excitation wavelength of 420 nm) of the effect of shearing on **1a** at room temperature (a), and at its various LC phases.

the maximum wavelength of the emission attributable to the $S_1 \rightarrow S_o$ relaxation in the shear-induced phase (λ_{max} = 623 nm) is blue-shifted by 30 nm relative to that in the Col_{h1} phase (Fig. 5a, right) while maintaining the absolute fluorescent quantum yield of 2% (see ESI,† Fig. S10). Moreover, the emission spectrum in the shear-induced phase at 25 °C (Fig. 5a, right) is found to be close to those in the Col_{h2} phase (λ_{max} = 611 nm) at 125 °C and in the isotropic liquid phase (λ_{max} = 604 nm) at 150 °C, as shown in Fig. 5b, right. From these results, we consider that the application of shear force to the Col_{h1} phase of **1a** may induce disorder in the columnar stacking structure of the X-shaped molecule.

Further investigation of the shear-induced LC phase of **1a** was performed. The thermal properties of the original LC sample and the sheared sample of **1a** were characterised by DSC heating traces (Fig. 6a). It is observed that the sheared sample exhibits two distinct peaks at 132 and 136 °C, with transition enthalpies of 14 and 1 kJ mol^{-1}, respectively. The total transition enthalpy from the shear-induced Col_h phase to the isotropic state is considerably lower than the transition enthalpy from the Col_{h1} phase to the isotropic state of another sample of **1a** that is not subject to shearing (30 kJ mol^{-1}). This result suggests that shearing of the LC sample causes a disorder in the molecular arrangement. We suspect that the broad peak at 132 °C in the DSC trace of the shear-induced phase is due to the inherently incomplete shearing process.

Furthermore, WAXD pattern of the sheared sample (Fig. 6b) shows only a broad peak at 47.7 Å (100), suggesting a new shear-induced Col phase. Assuming that the hexagonal lattice is maintained, the lattice parameter a of this disordered Col_h phase is calculated to be 55.5 Å, which is noticeably larger than that of Col_{h1} and Col_{h2} phases as shown in Table 1.

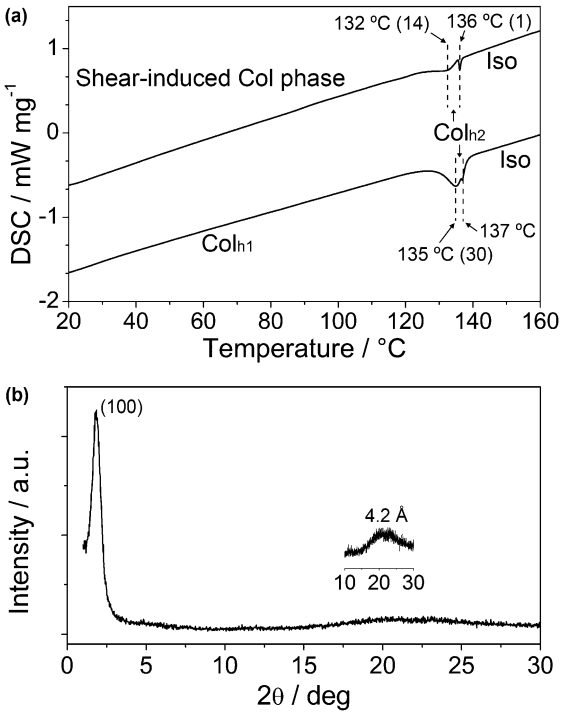

Fig. 6 The DSC traces of a sample of **1a** that is subject to shearing, and another sample that is cooled from an isotropic state to form the Col_{h2} phase (a). The heating rate is 10 K min^{-1} with transition enthalpies (kJ mol^{-1}) shown in parentheses. The WAXD pattern of the sheared-induced Col phase of **1a** (b) at room temperature.

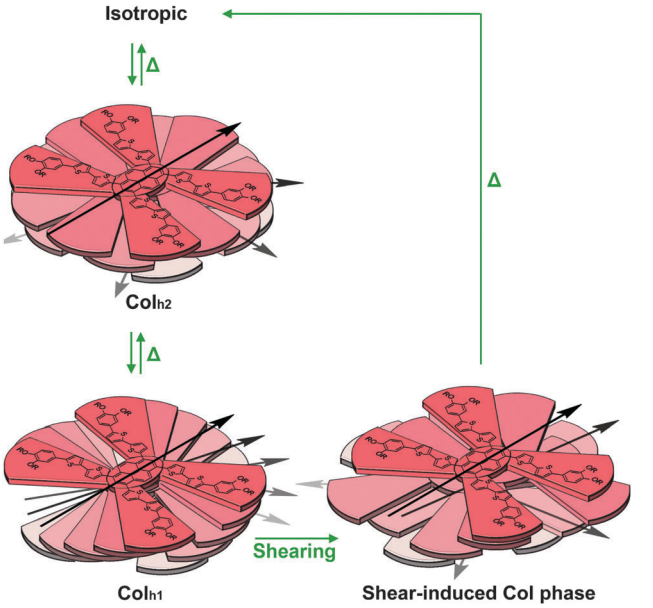

Fig. 7 The proposed transition scheme and intermolecular stacking arrangement of **1a** in the Col_{h1} phase, Col_{h2} phase and the shear-induced Col phase. The alkyl chains are omitted for clarity.

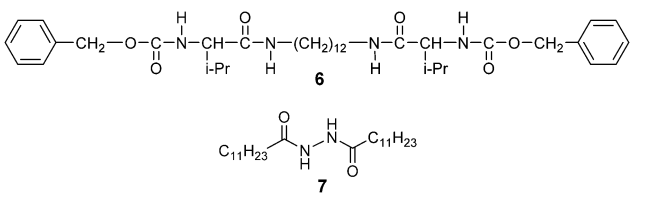

Scheme 3 The molecular structures of the gelator candidates employed.

From these observations, we propose that in the Col_{h1} phase, cofacial columnar stacks are formed with the individual X-shaped molecules of **1a** rotated with an angle of about 15°, forming a helical packing structure (Fig. 7). This assembly was found to exhibit higher stabilisation energy.[63] The blue-shift in the emission spectrum for the transition from the Col_{h1} phase to the Col_{h2} phase can be explained by the decreased inter-chromophoric interactions,[64] which is evident by another blue-shift for the transition to the isotropic state. Based on these results, it can be deduced that **1a** in the Col_{h2} phase presumably adopts a less cofacial stacking configuration with the X-shaped molecules rotated at a larger acute angle. (Fig. 7)

It is proposed that the mechanochromic response exhibited for compound **1a** can be explained in a similar way. The mechanical shearing force on **1a** disrupts the ordered arrangement of the aromatic cores, causing the sheared sample to adopt a new disordered Col phase, and resulting in lesser intermolecular π–π interactions. Consequently, a visible blue-shift in the fluorescence spectra is observed.

As for compound **1b**, shearing causes no observable change in the fluorescent properties. This can be attributed to the more rigid Col_r phase as compared to the Col_h phase.

LC gel properties

Incorporation of self-assembled fibres into the π-conjugated LC molecules is one approach to increase the hole mobility.[65–71] We intend to investigate the influence on photoconductivities by the introduction of fibrous networks into the X-shaped liquid crystals. In our previous studies, triphenylene-based liquid crystals were found to form LC gels with gelator **6**[71] (Scheme 3). However in the case of compound **1a**, the introduction of gelator **6** forms a macroscopically phase-separated mixture under the POM and scanning electron microscope (SEM) observations (see ESI,† Fig. S11). Compound **7** was thus employed in our study as it was known to exhibit good gelation properties in common organic solvents.[72]

The formation of a LC gel is achieved for compound **1a** with 3 weight% of gelator **7**. Upon cooling the mixture from the isotropic states, fibrous aggregates of **7** are first formed in the liquid of **1a**. Upon subsequent cooling, the orientation of the LC domains of **1a** along the fibrous network is observed under POM (Fig. 8a). The xerogel also reveals the fibrous network under SEM (Fig. 8b). The fibrous network is also observed by the introduction of gelator **7** into compound **1b** (see ESI,† Fig. S12).

The hole mobilities of LC gels of **1a** and **1b** with 3 weight% of gelator **7** are measured at varying temperatures and compared to their pure counterparts. For the LC gel of **1a**, consistently higher hole mobility was observed as compared to pure **1a**

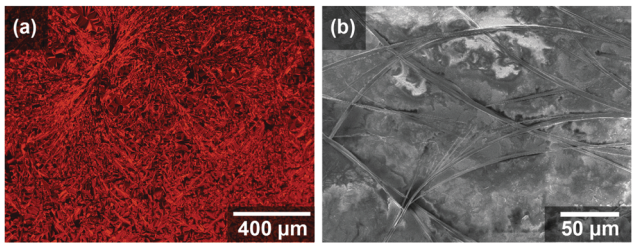

Fig. 8 The images of the LC gel of liquid crystal **1a** and gelator **7** upon cooling from the isotropic state to 125 °C under POM (a), and the fibrous structure of the xerogel under SEM (b).

(see ESI,† Fig. S13). At 117 °C, the LC gel shows a maximum hole mobility of 8.4×10^{-4} cm^2 V^{-1} s^{-1}, almost double of that of pure **1a**. In contrast, hole mobility of the LC gel of **1b** shows no significant difference as compared to pure **1b** (see ESI,† Fig. S14). In our previous studies, a significant increase in hole mobility was observed for the LC gels of triphenylene molecules, which could be attributed to the alignment of the liquid crystal on the fibrous structure that presumably suppresses the fluctuation of the molecular assembly of LC molecules.[68,71] The observations in this study suggest that the gelation exerted a smaller effect on the fluctuation of the X-shaped molecule **1b** as compared to **1a**, suggesting a more rigid stacking structure in the Col_t and Col_r phases of **1b** as compared to the Col_h phases of **1a**.

Conclusion

We have demonstrated that pyrene–oligothiophene based X-shaped molecules of **1a** and **1b** are capable of forming Col_h and Col_r phases over a wide range of temperature, including room temperature. TOF photoconductivity measurements reveal that the Col_h and Col_r phases of **1a** and **1b** show modest hole carrier transport in the order of 10^{-4} to 10^{-5} cm^2 V^{-1} s^{-1}. Compound **1a** exhibits mechano-sensitive photoluminescence properties, and the possible intermolecular configurations in different columnar phases have been elucidated. The introduction of a fibrous network also causes a small increase in hole mobility for **1a**. This simple strategy for the preparation of new and multi-functional liquid-crystalline pyrene–oligothiophene based X-shaped molecules would potentially contribute to the growing field of organic electronics.

Acknowledgements

This study was partially supported by Grant-in-Aid for Scientific Research A (KAKENHI 23245030 for T. K.) and Scientific Research on Innovative Area (Stimuli-responsive Chemical Species, KAKENHI 15H00921 for M. Y.) from the Ministry of Education, Culture, Sports, Science and Technology of Japan (MEXT). K. P. G. is grateful for the support by MEXT on his research and pursue of graduate degrees in the University of Tokyo.

Notes and references

1 *Chemistry of Discotic Liquid Crystals: From Monomers to Polymers*, ed. S. Kumar, Taylor and Francis, CRC Press, Boca Raton, FL, 2011.
2 *Handbook of Liquid Crystals*, ed. J. W. Goodby, P. J. Collings, T. Kato, C. Tschierske, H. Gleeson and P. Raynes, Wiley-VCH, Weinheim, Germany, 2nd edn, 2014.
3 W. Pisula and K. Müllen, in *Handbook of Liquid Crystals*, ed. J. W. Goodby, P. J. Collings, T. Kato, C. Tschierske, H. Gleeson and P. Raynes, Wiley-VCH, Weinheim, Germany, 2nd edn, 2014, ch. 20, vol. 8, pp. 627–673.
4 M. Funahashi, T. Yasuda and T. Kato, in *Handbook of Liquid Crystals*, ed. J. W. Goodby, P. J. Collings, T. Kato, C. Tschierske, H. Gleeson and P. Raynes, Wiley-VCH, Weinheim, Germany, 2nd edn, 2014, ch. 21, vol. 8, pp. 675–708.
5 N. Boden, R. J. Bushby and J. Clements, *J. Chem. Phys.*, 1993, **98**, 5920–5931.
6 D. Adam, P. Schuhmacher, J. Simmerer, L. Haussling, K. Siemensmeyer, K. H. Etzbachi, H. Ringsdorf and D. Haarer, *Nature*, 1994, **371**, 141–143.
7 F. J. M. Hoeben, P. Jonkheijm, E. W. Meijer and A. P. H. J. Schenning, *Chem. Rev.*, 2005, **105**, 1491–1546.
8 S. Kumar, *Chem. Soc. Rev.*, 2006, **35**, 83–109.
9 J. Wu, W. Pisula and K. Müllen, *Chem. Rev.*, 2007, **107**, 718–747.
10 S. Sergeyev, W. Pisula and Y. H. Geerts, *Chem. Soc. Rev.*, 2007, **36**, 1902–1929.
11 M. O'Neill and S. M. Kelly, *Adv. Mater.*, 2011, **23**, 566–584.
12 R. J. Bushby and K. Kawata, *Liq. Cryst.*, 2011, **38**, 1415–1426.
13 S. Kumar, *Isr. J. Chem.*, 2012, **52**, 820–829.
14 S. Kumar, *NPG Asia Mater.*, 2014, **6**, e82.
15 T. Wohrle, I. Wurzbach, J. Kirres, A. Kostidou, N. Kapernaum, J. Litterscheidt, J. C. Haenle, P. Staffeld, A. Baro, F. Giesselmann and S. Laschat, *Chem. Rev.*, 2016, **116**, 1139–1241.
16 V. Percec, M. Glodde, T. K. Bera, Y. Miura, I. Shiyanovskaya, K. D. Singer, V. S. K. Balagurusamy, P. A. Heiney, I. Schnell, A. Rapp, H. W. Spiess, S. D. Hudson and H. Duan, *Nature*, 2002, **417**, 384–387.
17 J. Wu, M. D. Watson, L. Zhang, Z. Wang and K. Müllen, *J. Am. Chem. Soc.*, 2004, **126**, 177–186.
18 M. G. Debije, J. Piris, M. P. de Haas, J. M. Warman, Ž. Tomović, C. D. Simpson, M. D. Watson and K. Müllen, *J. Am. Chem. Soc.*, 2004, **126**, 4641–4645.
19 H. Iino, J.-i. Hanna, R. J. Bushby, B. Movaghar, B. J. Whitaker and M. J. Cook, *Appl. Phys. Lett.*, 2005, **87**, 132102.
20 M. J. Sienkowska, H. Monobe, P. Kaszynski and Y. Shimizu, *J. Mater. Chem.*, 2007, **17**, 1392–1398.
21 X. Feng, V. Marcon, W. Pisula, M. R. Hansen, J. Kirkpatrick, F. Grozema, D. Andrienko, K. Kremer and K. Mullen, *Nat. Mater.*, 2009, **8**, 421–426.
22 S. Diring, F. Camerel, B. Donnio, T. Dintzer, S. Toffanin, R. Capelli, M. Muccini and R. Ziessel, *J. Am. Chem. Soc.*, 2009, **131**, 18177–18185.

23 B. Zhao, B. Liu, R. Q. Png, K. Zhang, K. A. Lim, J. Luo, J. Shao, P. K. H. Ho, C. Chi and J. Wu, *Chem. Mater.*, 2010, **22**, 435–449.
24 M.-C. Tzeng, S.-C. Liao, T.-H. Chang, S.-C. Yang, M.-W. Weng, H.-C. Yang, M. Y. Chiang, Z. Kai, J. Wu and C. W. Ong, *J. Mater. Chem.*, 2011, **21**, 1704–1712.
25 T. Hirose, Y. Shibano, Y. Miyazaki, N. Sogoshi, S. Nakabayashi and M. Yasutake, *Mol. Cryst. Liq. Cryst.*, 2011, **534**, 81–92.
26 E. Venuti, R. G. Della Valle, I. Bilotti, A. Brillante, M. Cavallini, A. Calò and Y. H. Geerts, *J. Phys. Chem. C*, 2011, **115**, 12150–12157.
27 Q. Xiao, T. Sakurai, T. Fukino, K. Akaike, Y. Honsho, A. Saeki, S. Seki, K. Kato, M. Takata and T. Aida, *J. Am. Chem. Soc.*, 2013, **135**, 18268–18271.
28 T. Hirose, H. Takai, M. Watabe, H. Minamikawa, T. Tachikawa, K. Kodama and M. Yasutake, *Tetrahedron*, 2014, **70**, 5100–5108.
29 S. R. McLaren, D. J. Tate, O. R. Lozman, G. H. Mehl and R. J. Bushby, *J. Mater. Chem. C*, 2015, **3**, 5754–5763.
30 T. Kushida, A. Shuto, M. Yoshio, T. Kato and S. Yamaguchi, *Angew. Chem., Int. Ed.*, 2015, **54**, 6922–6925.
31 A. Bacher, I. Bleyl, C. H. Erdelen, D. Haarer, W. Paulus and H.-W. Schmidt, *Adv. Mater.*, 1997, **9**, 1031–1035.
32 T. Hassheider, S. A. Benning, H.-S. Kitzerow, M.-F. Achard and H. Bock, *Angew. Chem., Int. Ed.*, 2001, **40**, 2060–2063.
33 A. M. van de Craats, N. Stutzmann, O. Bunk, M. M. Nielsen, M. Watson, K. Müllen, H. D. Chanzy, H. Sirringhaus and R. H. Friend, *Adv. Mater.*, 2003, **15**, 495–499.
34 I. O. Shklyarevskiy, P. Jonkheijm, N. Stutzmann, D. Wasserberg, H. J. Wondergem, P. C. M. Christianen, A. P. H. J. Schenning, D. M. de Leeuw, Ž. Tomović, J. Wu, K. Müllen and J. C. Maan, *J. Am. Chem. Soc.*, 2005, **127**, 16233–16237.
35 B. Mukherjee and M. Mukherjee, *Org. Electron.*, 2009, **10**, 1282–1287.
36 L. Schmidt-Mende, A. Fechtenkötter, K. Müllen, E. Moons, R. H. Friend and J. D. MacKenzie, *Science*, 2001, **293**, 1119–1122.
37 J. L. Li, M. Kastler, W. Pisula, J. W. F. Robertson, D. Wasserfallen, A. C. Grimsdale, J. S. Wu and K. Müllen, *Adv. Funct. Mater.*, 2007, **17**, 2528–2533.
38 K. Takemoto, M. Karasawa and M. Kimura, *ACS Appl. Mater. Interfaces*, 2012, **4**, 6289–6294.
39 L. Li, S. W. Kang, J. Harden, Q. Sun, X. Zhou, L. Dai, A. Jakli, S. Kumar and Q. Li, *Liq. Cryst.*, 2008, **35**, 233–239.
40 M. Funahashi and J.-i. Hanna, *Appl. Phys. Lett.*, 2000, **76**, 2574–2576.
41 M. Funahashi and J. I. Hanna, *Adv. Mater.*, 2005, **17**, 594–598.
42 M. P. Aldred, A. E. A. Contoret, S. R. Farrar, S. M. Kelly, D. Mathieson, M. O'Neill, W. C. Tsoi and P. Vlachos, *Adv. Mater.*, 2005, **17**, 1368–1372.
43 A. J. J. M. van Breemen, P. T. Herwig, C. H. T. Chlon, J. Sweelssen, H. F. M. Schoo, S. Setayesh, W. M. Hardeman, C. A. Martin, D. M. de Leeuw, J. J. P. Valeton, C. W. M. Bastiaansen, D. J. Broer, A. R. Popa-Merticaru and S. C. J. Meskers, *J. Am. Chem. Soc.*, 2006, **128**, 2336–2345.
44 M. Funahashi, F. Zhang and N. Tamaoki, *Adv. Mater.*, 2007, **19**, 353–358.
45 F. Zhang, M. Funahashi and N. Tamaoki, *Org. Electron.*, 2010, **11**, 363–368.
46 X. Zhang, L. J. Richter, D. M. DeLongchamp, R. J. Kline, M. R. Hammond, I. McCulloch, M. Heeney, R. S. Ashraf, J. N. Smith, T. D. Anthopoulos, B. Schroeder, Y. H. Geerts, D. A. Fischer and M. F. Toney, *J. Am. Chem. Soc.*, 2011, **133**, 15073–15084.
47 M. Funahashi, F. Zhang, N. Tamaoki and J.-i. Hanna, *ChemPhysChem*, 2008, **9**, 1465–1473.
48 K. Sun, Z. Xiao, S. Lu, W. Zajaczkowski, W. Pisula, E. Hanssen, J. M. White, R. M. Williamson, J. Subbiah, J. Ouyang, A. B. Holmes, W. W. H. Wong and D. J. Jones, *Nat. Commun*, 2015, **6**, 6013.
49 T. Yasuda, K. Kishimoto and T. Kato, *Chem. Commun.*, 2006, 3399–3401.
50 T. Yasuda, H. Ooi, J. Morita, Y. Akama, K. Minoura, M. Funahashi, T. Shimomura and T. Kato, *Adv. Funct. Mater.*, 2009, **19**, 411–419.
51 T. Yasuda, T. Shimizu, F. Liu, G. Ungar and T. Kato, *J. Am. Chem. Soc.*, 2011, **133**, 13437–13444.
52 Y. Sagara and T. Kato, *Angew. Chem., Int. Ed.*, 2008, **47**, 5175–5178.
53 Y. Sagara and T. Kato, *Nat. Chem.*, 2009, **1**, 605–610.
54 Y. Sagara, S. Yamane, T. Mutai, K. Araki and T. Kato, *Adv. Funct. Mater.*, 2009, **19**, 1869–1875.
55 M. Mitani, S. Yamane, M. Yoshio, M. Funahashi and T. Kato, *Mol. Cryst. Liq. Cryst.*, 2014, **594**, 112–121.
56 M. Mitani, S. Ogata, S. Yamane, M. Yoshio, M. Hasegawa and T. Kato, *J. Mater. Chem. C*, 2016, **4**, 2752–2760.
57 Z. Chi, X. Zhang, B. Xu, X. Zhou, C. Ma, Y. Zhang, S. Liu and J. Xu, *Chem. Soc. Rev.*, 2012, **41**, 3878–3896.
58 C. Löwe and C. Weder, *Adv. Mater.*, 2002, **14**, 1625–1629.
59 J. Kunzelman, M. Kinami, B. R. Crenshaw, J. D. Protasiewicz and C. Weder, *Adv. Mater.*, 2008, **20**, 119–122.
60 G. Zhang, J. Lu, M. Sabat and C. L. Fraser, *J. Am. Chem. Soc.*, 2010, **132**, 2160–2162.
61 T. Ishiyama, J. Takagi, Y. Yonekawa, J. F. Hartwig and N. Miyaura, *Adv. Synth. Catal.*, 2003, **345**, 1103–1106.
62 K. R. Idzik, P. J. Cywinski, W. Kuznik, J. Frydel, T. Licha and T. Ratajczyk, *Phys. Chem. Chem. Phys.*, 2015, **17**, 22758–22769.
63 V. de Halleux, J. P. Calbert, P. Brocorens, J. Cornil, J. P. Declercq, J. L. Brédas and Y. Geerts, *Adv. Funct. Mater.*, 2004, **14**, 649–659.
64 A. Hayer, V. de Halleux, A. Köhler, A. El-Garoughy, E. W. Meijer, J. Barberá, J. Tant, J. Levin, M. Lehmann, J. Gierschner, J. Cornil and Y. H. Geerts, *J. Phys. Chem. B*, 2006, **110**, 7653–7659.
65 T. Kato, N. Mizoshita and K. Kishimoto, *Angew. Chem., Int. Ed.*, 2006, **45**, 38–68.
66 T. Kato, Y. Hirai, S. Nakaso and M. Moriyama, *Chem. Soc. Rev.*, 2007, **36**, 1857–1867.
67 T. Kato, T. Yasuda, Y. Kamikawa and M. Yoshio, *Chem. Commun.*, 2009, 729–739.

68 T. Kato and K. Tanabe, *Chem. Lett.*, 2009, **38**, 634–639.
69 N. Mizoshita, H. Monobe, M. Inoue, M. Ukon, T. Watanabe, Y. Shimizu, K. Hanabusa and T. Kato, *Chem. Commun.*, 2002, 428–429.
70 M. Moriyama, N. Mizoshita and T. Kato, *Polym. J.*, 2004, **36**, 661–664.
71 Y. Hirai, H. Monobe, N. Mizoshita, M. Moriyama, K. Hanabusa, Y. Shimizu and T. Kato, *Adv. Funct. Mater.*, 2008, **18**, 1668–1675.
72 K. Tomioka, T. Sumiyoshi, S. Narui, Y. Nagaoka, A. Iida, Y. Miwa, T. Taga, M. Nakano and T. Handa, *J. Am. Chem. Soc.*, 2001, **123**, 11817–11818.